Nature-inspired geometrical design of a chemical reactor

Elisa Magnanelli[a,*], Simon Birger Byremo Solberg[b], Signe Kjelstrup[b]

[a] *SINTEF Energy Research, Sem Sælands vei 11, 7465 Trondheim, Norway*
[b] *PoreLab, Department of Chemistry, NTNU - Norwegian University of Science and Technology, 7491 Trondheim, Norway*

Abstract

We explore the possibility to actively use the system geometry to search for states of minimum entropy production in a chemical reactor. This idea is inspired by the energy-efficient mass and energy transfer that takes place in the reindeer nose thanks to its complex geometry. A cylindrical plug-flow reactor for oxidation of sulfur dioxide is used as example, while optimal control theory is used to formulate the problem. We hypothesize that the nasal anatomy of the reindeer has evolved to its present shape to help reducing energy dissipation during respiration in extreme ambient temperatures.

A comparable optimal diameter-profile in the plug-flow reactor resulted in 11% reduction of the total entropy production, compared to a cylindrical reference reactor. With, in addition, an optimal reactor length, the reduction is 16%. These reductions are largely due to reductions in viscous dissipation. In practice, this translates into smaller pressure drops across the system, which reduce the loads of upstream/downstream compressors. Moreover, the peak in the temperature profile was reduced with respect to that obtained by controlling the temperature of the cooling medium.

With today's technological solutions, the optimal diameter profile might be easier to realize than other optimal control strategies. The possible gains from this first example are encouraging, and may serve as inspiration for further applications.

Keywords: Optimal control theory, Entropy production minimization, Chemical reactors

1. Introduction

Over the last decades, much work has been done in the field of entropy production minimization for various kinds of process units [1–4]. By identifying where and how energy is dissipated in a process, we can in turn apply measures to reduce dissipation, see Ref. [5] for a review. While systematic improvements have yet to be carried out in practice, several studies on chemical reactors have been performed demonstrating that possible gains are significant [6, 7].

In search of new ways to improve the energy efficiency of chemical reactors, the plug-flow reactor has often been used as a simple model to minimize entropy production. Both exothermic and endothermic reactions have been studied, for instance oxidation of sulfur dioxide (SO_2) [6], ammonia production [8], methanol synthesis [9], propane dehydrogenation [10], steam reforming [11], and hydrogen production [12]. Different ways of improving reactors' energy efficiency have been explored, such as optimal control of the cooling medium temperature [6] and of the catalyst distribution [11], or reconfiguration of the process flow diagrams [5]. All different approaches have provided insight on the efficient operation and design of the process. However, such measures might be difficult to realize in practice. As an example, Johannessen *et al.* noted that an optimal ambient coolant temperature-profile might lead to potential issues due to catalyst deactivation and process stability [6]. In the effort to reduce energy dissipation in this particular system, other control variables may therefore be of interest.

Many interesting designs and patterns are found in nature, which respond to principles of efficiency and functionality [13]. In arctic regions animals show remarkable adaptations to the cold climate. An especially interesting example is the nasal anatomy of reindeer (*Rangifer tarandus*), which features a complex spiral structure [14]. Using a computational model, it has been shown that the nasal geometry of the reindeer contributes to a significant reduction in total entropy production of respiration, compared to a simple cylindrical nasal geometry [15]. Despite the extreme climate, physiology allows the animal to maintain its temperature nearly constant, and it appears that its nasal geometry contributes to this by reducing energy and water dissipation during respiration.

An analogy can be established between the evolution of the reindeer nose and optimization studies on chemical reactors. In both cases, the scope is to control the driving forces across the system to reduce dissipation. However, the ways the two problems are solved are different. In earlier works on reactors for SO_2 oxidation, driving forces have been controlled by controlling the temperature of the coolant [6]. However, due to physiological constraints, in the reindeer nose the temperature of the heating medium (i.e. the reindeer blood) cannot be let free to vary. In the reindeer nose driving forces are instead controlled through a varying geometry.

Coppens [16] has proposed nature-inspired chemical engineering as a useful discipline in a resource limited world. By taking inspiration from the reindeer nose, in the present work

*Corresponding author
Email address: elisa.magnanelli@sintef.no (Elisa Magnanelli)

we explore the possibility of reducing dissipation in a SO_2 plug flow reactor by optimizing its geometry. Observations on the importance of water recovery during reindeer respiration has already served as inspiration for a closer analysis of heat and mass exchangers in ventilation [17], and further observations on the complex reindeer nose structure could also have implications for reactor design. We hypothesize that *it is possible to reduce the total entropy production in the reactor by varying the reactor geometry*, while keeping the production of the reactor constant. With technological advances in 3D printing, a geometrical optimization could represent a more practical strategy than to use the coolant temperature as a control variable. Indeed, temperature control of the cooling medium can be practically done only in a discrete way, by using different cooling media in different sections along the reactor [18]. Under these premises, in the present work we will follow a "reindeer approach" in the optimization problem.

The task of finding the geometrical structure that reduces the entropy production can be formulated by optimal control theory. The general optimization procedure has been previously described in literature [6]. The resulting reactor diameter profile and the possibility of choosing a non-circular geometry of cross-sections will be discussed, and the results will be compared with those previously obtained from coolant temperature optimization [6].

2. The system

Figure 1 depicts a schematic representation of a tubular reactor for oxidation of SO_2, which has been earlier accurately described [6]. A gas mixture of SO_2, O_2, SO_3 and N_2 enters the reactor on the left side. The tubular reactor geometry is characterized by the diameter, D, cross-sectional area, A, perimeter, γ, and length, L, as illustrated in Fig. 1. As a reference case to compare the optimization results with, we use a reactor where the geometry is uniform along the length of the reactor (the adopted geometrical parameters are presented in Appendix A).

The reactor is filled with a packed bed of catalytic particles. As SO_2 comes in contact with the catalyst, it is oxidized according to the stoichiometric reaction:

$$SO_2 + \tfrac{1}{2}O_2 = SO_3$$

The catalyst bed is made up by spherical particles of constant density, ρ_B, and diameter, D_p, resulting in a constant void fraction, ϵ. The overall density of catalyst in the reactor is then given by:

$$\rho_{\text{eff}} = \rho_B\,(1-\epsilon) \tag{1}$$

Since the oxidation reaction is exothermic, active cooling is provided to the reactor by a boiling cooling medium (i.e. at constant temperature, T_{amb}), which surrounds the walls of the reactor.

In the description of the reactor, some simplifying assumptions are made:

- the reactive flow within the tubular reactor is described as plug-flow, which implies that radial gradients are neglected, the radial gas velocity profile is flat, and the process is at steady state;
- heterogeneous effects due to diffusion and reactions in the catalyst particles are neglected (pseudo-homogeneous model [19]);
- diffusive fluxes along the axial direction are neglected, as they are small in comparison to the convective flow;
- ideal gas law is used to describe the behaviour of the gas mixture.

By applying these assumptions the conservation equations which govern the behaviour of the system can be formulated as described in Section 3.

3. Theoretical formulation

In Section 3.1, the equations that describe the system behavior are presented. In Section 3.2, we define the entropy production of the system, which is the objective function for the optimal control problems described in Section 3.3.

3.1. Conservation equations

As the gas mixture flows through the catalytic bed, SO_2 is oxidized releasing a large amount of heat. At the same time, the reactor exchanges heat with a cooling medium, which prevents an excessive rise in temperature within the reactor. The energy balance can then be written as [6]:

$$\frac{\mathrm{d}T}{\mathrm{d}z} = \frac{\gamma' J_q' + A\rho_{\text{eff}}(-\Delta_r H) r_{SO_2}}{\sum_i F_i C_{p,i}} \tag{2}$$

where r_{SO_2} is the reaction rate per unit mass of catalyst, $\Delta_r H$ is the reaction enthalpy, $C_{p,i}$ is the heat capacity of component i, and $\gamma' = \gamma\sqrt{1+\frac{1}{4}\left(\frac{\mathrm{d}D}{\mathrm{d}z}\right)^2}$ is the perimeter multiplied by a factor that accounts for the curvature of the reactor outer surface when integrating along the z-coordinate. The measurable heat flux across the reactor wall, J_q', can be calculated as [20]:

$$J_q' = U\,(T_{\text{amb}} - T) \tag{3}$$

where U is the overall heat transfer coefficient. Appendix A contains additional information on the parameters used in Eq. 2.

The purpose of the reactor is to oxidize SO_2. The conversion of this component, ξ, can be written at any position along the z-coordinate as:

$$\xi = \frac{F^0_{SO_2} - F_{SO_2}}{F^0_{SO_2}} \tag{4}$$

where $F^0_{SO_2}$ is the molar flow rates of SO_2 at the inlet, while F_{SO_2} is the SO_2 molar flow rate at the consider position. The molar flow rate of component i, F_i, and the total molar flow rate, F_T, can be written in relation to the SO_2 molar flow rate as:

$$\begin{aligned} F_i &= F^0_{SO_2}\,(\theta_i + \nu_i\xi) \\ F_T &= F^0_{SO_2}\left(\theta_T + \xi\sum_i \nu_i\right) \end{aligned} \tag{5}$$

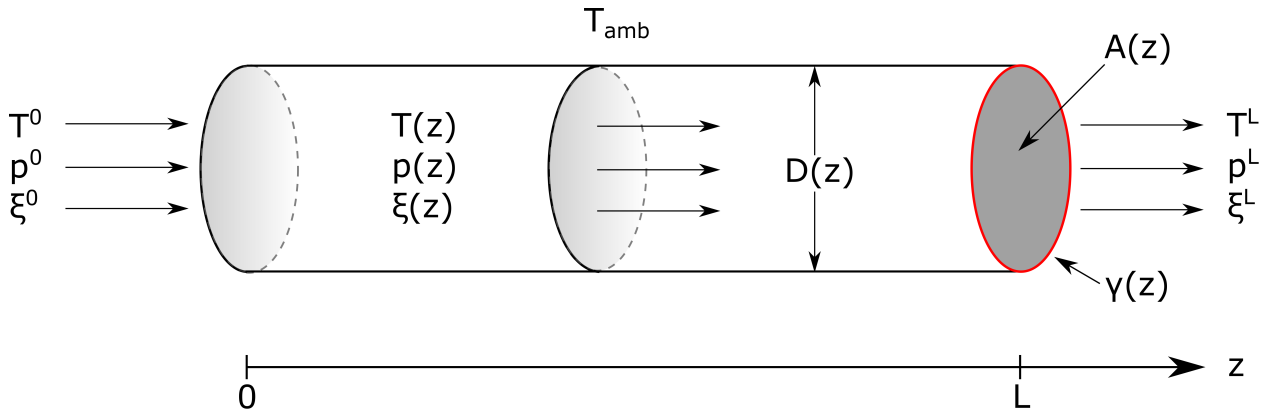

Figure 1: Sketch of the plug-flow reactor. Adapted from Ref. [6].

where ν_i, is the stoichiometric coefficient of component i in the oxidation reaction, and θ_i is defined as:

$$\theta_i = \frac{F_i^0}{F_{\mathrm{SO}_2}^0} \qquad \theta_T = \frac{F_T^0}{F_{\mathrm{SO}_2}^0} \tag{6}$$

Mole fractions of each component can then be determined using:

$$x_i = \frac{F_i}{F_T} = \frac{\theta_i + \nu_i \xi}{\theta_T + \xi \sum_i \nu_i} \tag{7}$$

The generalized mole balance for the reactive flow can be formulated in terms of the conversion as [6]:

$$\frac{\mathrm{d}\xi}{\mathrm{d}z} = \frac{A \rho_{\mathrm{eff}} r_{\mathrm{SO}_2}}{F_{\mathrm{SO}_2}^0} \tag{8}$$

The packed bed of particles offers a large resistance to the gas mixture flowing through the bed. The resulting pressure drop can be described by Ergun's equation [19, 21]

$$\frac{\mathrm{d}p}{\mathrm{d}z} = -\left(\alpha + \beta v\right) v \tag{9}$$

where v is the gas superficial velocity, and α and β are defined as [21]:

$$\alpha = \frac{150\mu}{D_p^2} \frac{(1-\epsilon)^2}{\epsilon^3} \qquad \beta = \frac{1.75\rho}{D_p} \frac{1-\epsilon}{\epsilon^3} \tag{10}$$

where μ is the gas viscosity, and ρ is the gas density. Since the reactive components are dilute in inert nitrogen gas, the difference between the molar average velocity and mass average velocity is small. The superficial gas velocity is the flow velocity that the gas would have if it occupied the whole reactor cross-section:

$$v = \frac{F_T}{A\rho} \qquad \rho = \frac{p M_w^T}{RT} \tag{11}$$

where M_w^T is the molecular weight of the gas mixture, and R is the universal gas constant.

3.2. The entropy production

The local entropy production in the plug-flow reactor has three contributions: entropy generated by heat transfer, viscous dissipation, and entropy produced by the chemical reaction. The entropy production per unit length of the plug-flow reactor is given by Johannessen *et al.* [6] as:

$$\sigma = \gamma' J_q' \left(\frac{1}{T_{\mathrm{amb}}} - \frac{1}{T}\right) + Av\left(-\frac{1}{T}\frac{\mathrm{d}p}{\mathrm{d}z}\right) + A\rho_{\mathrm{eff}} r_{\mathrm{SO}_2}\left(-\frac{\Delta_r G}{T}\right) \tag{12}$$

where $\Delta_r G$ is the reaction Gibbs energy. The total entropy production is found by integration of the local entropy production over the reactor length:

$$\Sigma_{\mathrm{irr}} = \int_0^L \sigma \mathrm{d}z = \Sigma_{\mathrm{irr,dT}} + \Sigma_{\mathrm{irr,dp}} + \Sigma_{\mathrm{irr},\Delta\mathrm{G}} \tag{13}$$

Since the system is in a steady state, the total entropy production can also be calculated from the entropy balance over the whole reactor:

$$\Sigma_{\mathrm{irr}} = F_T^{\mathrm{out}} S^{\mathrm{out}} - F_T^{\mathrm{in}} S^{\mathrm{in}} + \Delta S_{\mathrm{utility}} \tag{14}$$

where $\Delta S_{\mathrm{utility}}$ is the entropy change of the cooling utility, and S^{in} and S^{out} are the entropy of the inlet and outlet flow, respectively. In calculations, the results obtained by Eq. 13 and Eq. 14 can be compared to check the consistency of the model.

The entropy change of the utility is due to the heat exchanged with the reactor:

$$\Delta S_{\mathrm{utility}} = -\int_0^L \frac{\gamma' J_q'}{T_{\mathrm{amb}}} \mathrm{d}z \tag{15}$$

3.3. The optimization problem

The purpose of the optimization procedure is to find the reactor geometry which minimizes the total entropy production. Control on the geometry is done by letting the diameter of the reactor free to vary along the reactor length.

As presented in Section 3.1, the plug-flow reactor considered in this work is completely described by three state variables (i.e. T, ξ, and p), each of which is governed by a conservation equation (i.e. Eq. 2, Eq. 4, and Eq. 9). According to optimal control

theory, the Hamiltonian for the problem may be employed in the solution of the optimization problem [22, 23]:

$$H = \sigma + \lambda_T \frac{\gamma' J'_q + A\rho_{\text{eff}}(-\Delta_r H) r_{\text{SO}_2}}{\sum_i F_i C_{p,i}} - \lambda_p (\alpha + \beta v) v + \lambda_\xi \frac{A\rho_{\text{eff}} r_{\text{SO}_2}}{F^0_{\text{SO}_2}} \quad (16)$$

where H is the Hamiltonian of the control problem. The Hamiltonian consists of two contributions. The first contribution is given by the integrand of the objective function to be minimized (i.e. the integrand in Eq. 13). A second contribution is given by the sum of the product of the multipliers' functions (λ_T, λ_ξ, and λ_p) and the right-hand side of the governing equation of the respective state variable [22, 23].

According to optimal control theory, the necessary conditions for a minimum in the objective function are given by two differential equations for each of the state variables, and by one algebraic equation for each of the control variables [22, 23]. The differential equations are:

$$\frac{\mathrm{d}T}{\mathrm{d}z} = \frac{\partial H}{\partial \lambda_T} \quad (17)$$

$$\frac{\mathrm{d}p}{\mathrm{d}z} = \frac{\partial H}{\partial \lambda_p} \quad (18)$$

$$\frac{\mathrm{d}\xi}{\mathrm{d}z} = \frac{\partial H}{\partial \lambda_\xi} \quad (19)$$

$$\frac{\mathrm{d}\lambda_T}{\mathrm{d}z} = -\frac{\partial H}{\partial T} \quad (20)$$

$$\frac{\mathrm{d}\lambda_p}{\mathrm{d}z} = -\frac{\partial H}{\partial p} \quad (21)$$

$$\frac{\mathrm{d}\lambda_\xi}{\mathrm{d}z} = -\frac{\partial H}{\partial \xi} \quad (22)$$

The algebraic conditions are derived by differentiating the Hamiltonian with respect to the control variables [22, 23]. Thus, the algebraic conditions depend on the choice of the control variables.

In the present case, the algebraic condition is given as:

$$\frac{\partial H}{\partial D} = 0 \quad (23)$$

By carrying out the differentiation, Eq. 23 can be rewritten as:

$$\frac{\partial H}{\partial D} = \frac{\pi}{2} D\rho_{\text{eff}} r_{\text{SO}_2}\left(-\frac{\Delta_r G}{T}\right) + \frac{d\gamma'}{dD} J'_q \left(\frac{1}{T_{\text{amb}}} - \frac{1}{T}\right) + \lambda_T \frac{\frac{d\gamma'}{dD} J'_q + \frac{\pi}{2} D\rho_{\text{eff}}(-\Delta_r H) r_{\text{SO}_2}}{\sum_i F_i C_{p,i}} + \left(\lambda_p - \frac{F_T R}{p}\right)\left(\alpha \frac{2}{D} v + \beta \frac{4}{D} v^2\right) + \lambda_\xi \frac{\pi D \rho_{\text{eff}} r_{\text{SO}_2}}{2F^0_{\text{SO}_2}} = 0 \quad (24)$$

By solving Eq. 24 for D, the optimal diameter profile along the z-coordinate can be found.

As ,n additional case interesting to explore, we consider the system length as free to vary. According to optimal control theory [22], the optimal length of the system is in this case characterized by a terminal value of the Hamiltonian equal to zero:

$$H_{z=L} = 0 \quad (25)$$

3.4. Constraints

Constraints are necessary for an optimization procedure to be meaningful [6, 22]. Indeed, when no constraints are imposed, the optimization may lead to trivial solutions (e.g. a reactor with length equal to zero). The optimization problem is described by six differential equations (Eqs. 17-22), and thus six constraints are necessary. Such constraints are formulated in the form of boundary conditions.

Since the purpose of the reactor is to produce SO_3 from SO_2, we impose that the conversion at the inlet and outlet of the reactor is equal to that of the reference reactor with uniform geometry:

$$\xi^0 = 0 \qquad \text{and} \qquad \xi^L = \xi^L_{\text{ref}} \quad (26)$$

The four additional constraints are imposed on the inlet and outlet values of pressure and temperature, as [6]:

$$\begin{array}{llll} T^0 & \text{specified} & \text{or} & \lambda^0_T = 0 \\ T^L & \text{specified} & \text{or} & \lambda^L_T = 0 \\ p^0 & \text{specified} & \text{or} & \lambda^0_p = 0 \\ p^L & \text{specified} & \text{or} & \lambda^L_p = 0 \end{array} \quad (27)$$

If a boundary condition at the reactor inlet or outlet is specified, its value is equal to that of the reference reactor at that position. If the state variable is free to vary at that point, its Lagrange multiplier is instead equal to zero [6, 22]. We assume that all pressure and temperature values at inlet and outlet are fixed, with exception for the inlet pressure, which is let free to vary.

3.5. Investigated cases

In the present work, we consider and compare the results from three cases:

Reference: This is the reference case; a plug-flow reactor with uniform geometry profiles, and reactor parameters given by Fogler [20]. No variables are optimized, and this case gives the boundary conditions for the geometrical optimization.

(D)-optimal: Optimal case, where the diameter profile, D, is optimized to minimized entropy production. The reactor length, L, is fixed and equal to that of the reference reactor.

(D, L)-optimal: Optimal case, where the diameter profile, D, and the length of the reactor, L, are optimized to minimize entropy production.

(T_{amb})-optimal: Optimal case presented in Reference [6], where the temperature profile of the utilities, T_{amb}, is optimized to minimized entropy production. The reactor length, L, is fixed and equal to that of the reference reactor.

(T_{amb}, L)-optimal: Optimal case presented in Reference [6], where the temperature profile of the utilities, T_{amb}, and the length of the reactor, L, are optimized to minimize entropy production.

The initial conditions for the reference reactor are presented in Table 1.

Table 1: Initial conditions used in the reference reactor calculations [20].

	Value	Unit
T^0	777.78	K
p^0	202650	Pa
F_T^0	0.2149	mol s^{-1}
$x^0_{SO_2}$	0.11	-
$x^0_{O_2}$	0.10	-
$x^0_{SO_3}$	0.01	-
$x^0_{N_2}$	0.78	-

4. Solution procedure

For the reference case, the conservation equations (Eq. 2, 4 and 9) and the initial conditions given by Fogler (see Table 1) constitute an initial value problem (IVP). In MATLAB this problem is numerically integrated using the function **ode15s**.

In the optimization problems, constrains are specified at both ends of the system. This makes the problem a two-point boundary value problem (BVP), which cannot be solved by **ode15s**. The BVP can be solved numerically in MATLAB using the function **bvp4c**, which employs a collocation method. In order for the solver to converge, we must provide a reasonable guess of the problem solution. The MATLAB function **fmincon** is used to find suitable initial guesses for the state variable, control variable and Lagrange multiplier profiles. An initial guess on a coarse grid of roughly 25-50 points is sufficient for the solver to converge.

The algebraic relation which gives the diameter, Eq. 23, is a non-linear function, and is solved in MATLAB using the function **fsolve**. Equation 23 is solved for each point along the length of the reactor, and the resulting values of the diameter are used in the calculation of spatial gradients of state variables and Lagrange multipliers given in Eq. 17-22. A finite central difference scheme for MATLAB, developed by Johannessen *et al.*, is used to approximate spatial gradients of the Lagrange multipliers [6]. To summarize, the following computational procedure is used to solve the problem in MATLAB:

- The reference case IVP is solved using **ode15s**. Inlet and outlet boundary conditions from this case are subsequently used in the optimization.
- A numerical solution of the optimization problem is found using **fmincon**. Profiles of state variables, Lagrange multipliers and the control variable are used as an initial guesses for the analytic solution.
- A preliminary analytic solution of the optimization problem, where γ' is approximated to $\gamma' = \gamma$, is found using **bvp4c** and **fsolve** with suitable initial guesses.
- The exact analytic solution is found using **bvp4c** and **fsolve** in combination with an iterative procedure where the preliminary analytic solution is used to guess profiles of state variables and geometrical parameters.

When we also attempt to optimize the reactor length we require two more steps:

- Analytic solutions are found for different lengths, using the previous solution as an initial guess for the next optimization.
- Total entropy production and terminal value of the Hamiltonian may then be illustrated as a function of reactor length, and the optimal reactor length can be found.

The consistency of the thermodynamic model was checked by comparing the total entropy production obtained with Eq. 13, to the value obtained from Eq. 14. The difference between the two calculations was less than 1%, and became smaller as the accuracy of calculations was increased. An inlet mole fraction for SO_3 of $x^0_{SO_3} = 0.01$ was chosen instead of 0, to avoid problems with the numerical solution of the problem [6].

5. Results and Discussion

5.1. Entropy production

The purpose of the optimization procedures is to minimize the entropy production of the process. The total entropy production obtained in the considered cases is presented in Table 2. The results show that with the control of the diameter profile only ((D)-optimal), the total entropy production reduces by circa 11% with respect to the reference case, while the additional optimization of the reactor length allows us to obtain an overall entropy production reduction of 16%.

In both cases, the reduction in Σ_{irr} is due to reduction in the entropy production due to viscous dissipation and by heat transfer, while the contribution due to chemical reaction is slightly larger than in the reference case.

The reduction in entropy production is comparable to that obtained by Johannessen *et al.* [6] when optimizing the cooling medium temperature alone ((T_{amb})-optimal) or in combination with the reactor length ((T_{amb},L)-optimal. However, when T_{amb} is used as control variable in the optimization, most of the reduction in entropy production is due to the chemical reaction contribution, while the contribution due to viscous flow remains approximately the same.

5.2. Temperature profile across the reactor

Figure 2 presents the temperature profile in the reactor as a function of the normalized z-coordinate (i.e. the coordinate value divided by the length of reactor), for the different cases. In the reference reactor (dashed line), the temperature of the reacting mixture rises quickly as the gas enters the reactor, due to the oxidation reaction being exothermic. When most of the SO_2 has oxidized to SO_3, the reaction rate slows down and the temperature of the gas mixture starts decreasing, until it approaches that of the cooling medium that surrounds the reactor.

For the cases (D)-optimal and (D,L)-optimal, the shape of the temperature profile is very similar to that of the reference case. In (D)-optimal, the maximum temperature of the gas mixture is circa 10 K lower than in the reference case. A lower maximum temperature and a lower temperature variation within the system reduce thermal stresses on the reactor materials as well as contribute to the stability of the process.

Table 2: Total entropy production (J $K^{-1}s^{-1}$) for the reference, (D)-optimal and (D,L)-optimal. The percentage in parenthesis represent the reduction in entropy production obtained with respect to the reference case. Results from a previous work [6] for (T_{amb})-optimal and (T_{amb},L)-optimal are also reported for comparison.

	Reference	(D)-optimal	(D,L)-optimal	(T_{amb})-optimal	(T_{amb},L)-optimal
Σ_{irr}	1.4204	1.2644	1.1887	1.2555	1.0551
	(-)	(-11%)	(-16%)	(-10%)	(-24%)
$\Sigma_{irr,dT}$	0.4497	0.4082	0.4396	0.3929	0.2261
$\Sigma_{irr,dp}$	0.5615	0.4181	0.3429	0.5600	0.5631
$\Sigma_{irr,\Delta G}$	0.4048	0.4381	0.4062	0.3026	0.2660

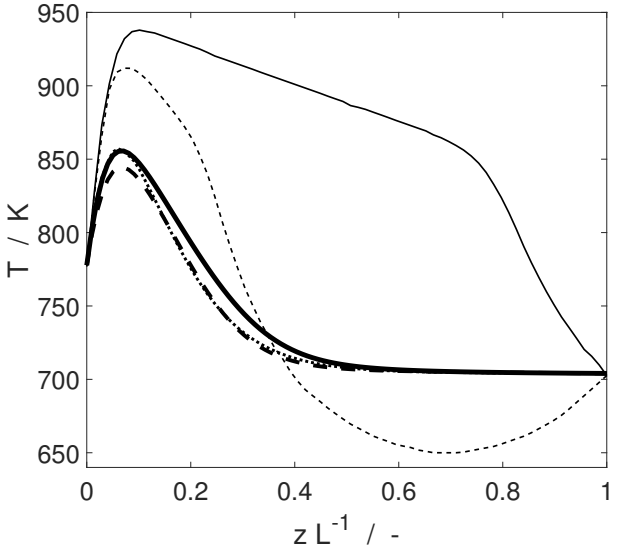

Figure 2: Temperature inside the reactor as a function of the scaled position, for the reference (dotted line), (D)-optimal (dashed thick line), (D,L)-optimal (solid thick line). Results from a previous work [6] for (T_{amb})-optimal (dashed thin line), (T_{amb},L)-optimal (solid thin line) are also reported for comparison.

On the other hand, the results obtained by control of the cooling medium temperature carried out by Johannessen *et al.* [6] show that in both (T_{amb})-optimal (dashed thin line) and in (T_{amb},L)-optimal (solid thin line) a much higher maximum temperature than the reference case is reached. The authors noted that in practice such a high temperature can cause catalyst deactivation, in addition to thermal stress to reactor materials [6].

Thus, while to optimize the cooling medium temperature does reduce the entropy production of the process (see Table 2, it might lead to stability problems. These problems are instead not encountered when the diameter profile is used as control variable.

5.3. The optimal geometry

Figure 3a shows how the perimeter of the reactor cross section varies in the difference cases. For both (D)-optimal (dotted line) and (D,L)-optimal (solid line), in the central part of the reactor the perimeter is much larger than the constant one of the reference case (dashed line).

Variation in the reactor diameter has several effects on the system. When the diameter is larger, contact area between the cooling medium and the reactor is larger and, thus, heat exchange is enhanced. At the same time, a larger diameter leads also to an increased volume of the reactor and catalyst, and therefore favours eventual reactions. Finally, as the cross section also increases with a larger diameter, the velocity of the gas mixture decreases, leading to lower viscous dissipation. It is therefore difficult to isolate the effect of reactor diameter variation on the different transport phenomena.

It is interesting to notice that the optimal geometrical profiles found through the optimization procedures have some similarities to that of the reindeer nose (Fig. 3b). Indeed, in both systems, the perimeter is smaller at the inlet and outlet, than it is in the middle. Near the inlet, where driving forces are larger for both systems, the cross-sectional area and perimeter are relatively small, while the gas velocity is high. The more symmetrical profile of the reindeer nose can be expected due to the fact that the air velocity changes direction during the breathing cycle. To reverse flow is not relevant for the reactor.

5.4. The optimal reactor length

The optimal reactor length was found by evaluating the total entropy production and the terminal Hamiltonian value for different reactor lengths. The total entropy production of the reactor as a function of reactor lengths is shown in Fig. 4, together with individual contributions to it. A reactor length of 4.76 m gave a minimum in the total entropy production.

Similar to variation in the diameter profile, variation in the reactor length has mainly an impact on the reduction of the viscous dissipation. By optimizing the reactor length, the viscous dissipation was further reduced by 5% compared to the optimal case with reference reactor length (see Table 2).

The contribution to entropy production due to chemical reaction only slightly increases, as L increases. The heat transfer contribution has also very small variation, but it shows an opposite trend than that of $\Sigma_{irr,\Delta G}$.

An interesting advantage of the (D,L)-optimal case is that this geometry lowers the total reactor volume with respect to (D)-optimal. Figure 5 shows how the total volume and surface area of the reactor vary as a function of the reactor length. Figure 5 shows that, when the diameter profile is optimized maintaining the same reactor length as the reference case, a 47% larger volume of catalyst is necessary than in the reference case. However, the reactor volume decreases as the reactor length decreases. In (D,L)-optimal case, only 13% extra catalyst is necessary with respect to the reference case.

Due to the high costs of catalyst, the increased catalyst volume is a drawback of the geometrical optimization. However, in the present work, the catalyst density has been considered uniform along the reactor. By introducing the catalyst density

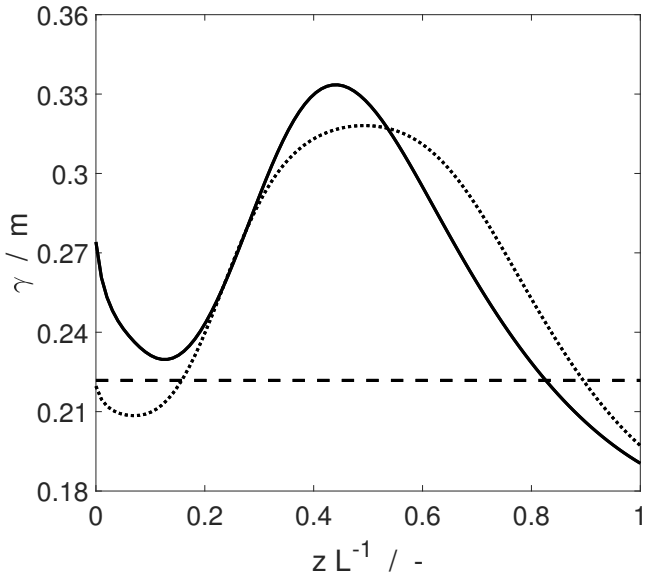

(a) Cross sectional perimeter of the reactor for the reference (dashed line), (D)-optimal (dotted line) and (D,L)-optimal (solid line).

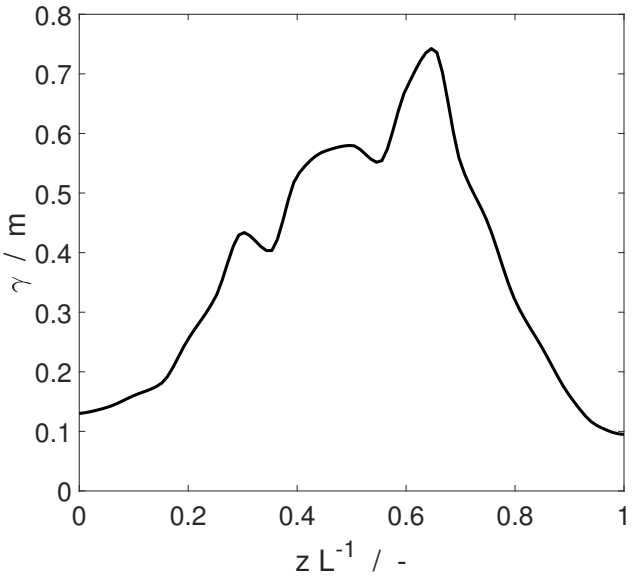

(b) Cross sectional perimeter of the reindeer nose [14].

Figure 3: Comparison between the cross sectional perimeter as a function of scaled position in the optimized reactor and in the reindeer nose.

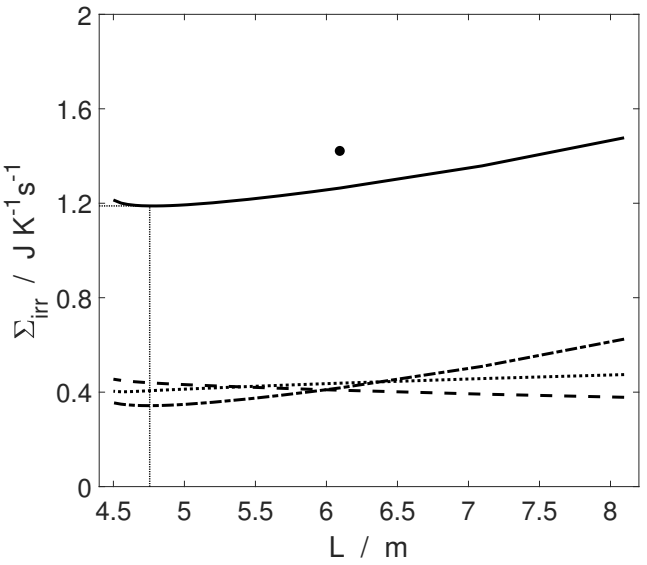

Figure 4: The total entropy production, Σ_{irr}, of the reference (circle) and of the optimal diameter reactor (solid line) a function of reactor length, L. The different contributions to the total entropy production are also shown: $\Sigma_{irr,dT}$ (dashed line), $\Sigma_{irr,dp}$ (dash-dotted line) and $\Sigma_{irr,\Delta G}$ (dotted line).The vertical line indicates the reactor length for which a minimum in entropy production is obtained.

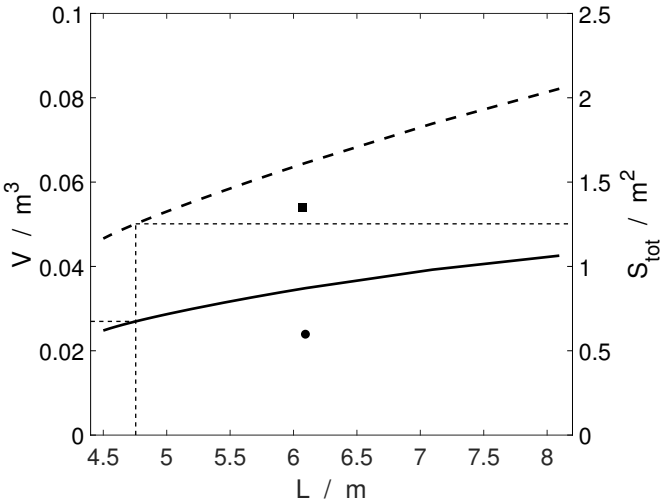

Figure 5: Total volume, V, of the reference (circle) and optimal diameter reactor (solid line), and total surface area, S_{tot}, of the reference (square) and of the optimal diameter reactor (dashed line) as functions of reactor length.). The vertical line indicates the reactor length for which a minimum in entropy production is obtained.

as an additional control variable, it might be possible to reduce the catalyst total volume below the reference one.

The total surface area of the reactor is also an important parameter. Figure 5 shows that the surface area decreases as the reactor length decreases. For a reactor length equal to the reference, the optimal reactor requires 19% larger surface area than the reference case. However, for the (D,L)-optimal case, the surface area is 7% lower than in the reference.

5.5. Practical considerations

As seen in Section 5.1, the entropy production reduction obtained through optimization of the reactor geometry, mainly leads to a reduction in viscous dissipation.

Figure 6 shows how the pressure varies along the reactor. A reduction in the viscous dissipation is directly related to a lower total pressure drop across the reactor. Since we let the inlet pressure free to vary, a lower pressure drop across the system results in a lower inlet pressure of the reacting mixture. From a practical point of view, a lower inlet pressure might lower the power requirements for compressors upstream the reactor,

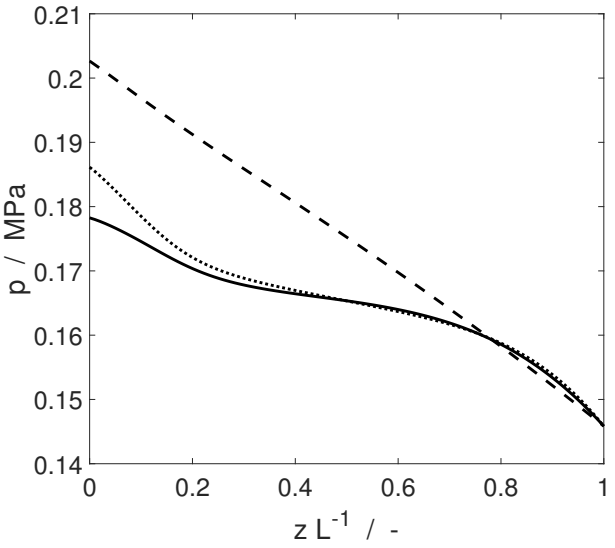

Figure 6: Pressure along the reactor as a function of the scaled position, for the reference (dashed line), (D)-optimal (dotted line), (D,L)-optimal (solid line).

leading to lower operation costs.

The practical realization of a reactor with varying diameter might be difficult to accomplish. Advances in 3D printing are however promising for the realization of such geometries. Nonetheless, production costs might be high to justify the reported increases in efficiency.

To further reduce energy dissipation, it might be interesting to explore how additional control variables might affect the results. Density distribution of the catalyst can provide a further way to control the chemical reaction driving forces.

5.6. Final remarks on the optimal geometry

Figure 7 shows a three dimensional representation of the optimized geometry.

In this work, we have optimized the diameter profile of the reactor, while maintaining the shape of the cross section circular. The resulting geometry was able to reduce the contributions to the entropy production due to viscous dissipation and, in smaller degree, due to heat transfer. On the other hand, the contribution due to reaction was slightly higher.

Nonetheless, as the complex geometry of the reindeer nose suggests, cross sectional shapes other than the circular one might allow for further reduction of energy dissipation. The reindeer nose is characterized by a shell-like structure [14], which makes it possible to decouple control of the cross-sectional area and perimeter of the nasal cavity. This allows for a better control of the thermodynamic driving forces. To take this into account, as a first simple example, an elliptic cross section could be considered, and its profile along the reactor optimized.

However, many other efficient designs can be found in nature, which could also be used as an inspiration for geometrical redesign. As an example, the complex lung airways are not only an efficient mass exchanger, but the pressure drop in them appears also optimally distributed [24].Thus, the fractal-like geometry of the lung could also represent an interesting geometry to study.

Figure 7: Three-dimensional of the reference reactor (bottom) and of the (D,L)-optimal reactor (top).

6. Conclusions and future work

The peculiar geometry of the reindeer nose was used as inspiration to find the minimum entropy production of a plug-flow reactor for SO_2-oxidation. The reactor diameter was used as control variable in the optimization procedure formulated by optimal control theory. We found that with the control of the diameter profile alone, the total entropy production reduces by circa 11% with respect to the reference case, while the additional optimization of the reactor length allowed us to obtain an overall entropy production reduction of 16%. In both cases, the reduction in Σ_{irr} was mainly due to reduction in the entropy production due to viscous dissipation, with a small contribution from heat transfer.

Differently from earlier works, the results of the optimization procedure did not lead to significant increase in the operating temperature. Thus, a practical realization of the optimal solution would not meet stability problems. Moreover, the optimal solution lead to a lower pressure drop across the system,

Quite interestingly, the optimal geometrical profile has some analogies to the one of the reindeer nose, with smaller perimeter at the inlet and outlet of the system, and larger perimeter in the central part. With today's technological solutions, the optimal diameter profile might be easier to realize than other optimal control strategies, such as control of the cooling medium temperature. The gains highlighted from this first example are encouraging, and may serve as inspiration for further applications.

The control of additional variables might further reduce process dissipation in future works. To separately control the perimeter and the cross sectional area of the reactor can lead to reduced entropy production. Moreover, the simultaneous control of geometry and distribution of catalyst may be of interest.

Acknowledgments

The authors gratefully acknowledge the financial support from the Research Council of Norway through its Centre of

Table A.3: Parameters for the tubular reactor [20]. T_{amb} is the cooling medium temperature, L_{ref} and D_{ref} are the length and diameter of the reference reactor, ϵ is the catalyst void fraction, ρ_B is the catalyst density, D_p is the catalyst particle diameter, U is the overall heat transfer coefficient, and μ is the gas viscosity.

	Value	Unit
T_{amb}	702.6	K
L_{ref}	6.096	m
D_{ref}	0.0706	m
ϵ	0.45	-
ρ_B	984.4	kg m^{-3}
D_p	$4.572 \cdot 10^{-3}$	m
U	56.783	J K^{-1} m^{-2} s^{-1}
μ	$3.7204 \cdot 10^{-5}$	kg m^{-1}s^{-1}

Excellence funding scheme, project number 262644, PoreLab, and through HighEFF, an 8-year Research Centre under the FME-scheme (Centre for Environment-friendly Energy Research, 257632/E20).

Appendix A. Thermodynamic parameters and relations

Reactor parameters and gas mixture properties are summarized in Table A.3. The cooling medium temperature, void fraction, catalyst density, catalyst particle diameter, and gas viscosity are constant along the length of the reactor, and are the same for the reference and the optimized reactor.

The reaction rate of SO_2 is described in the literature by using an empiric relation [20]:

$$r_{SO_2} = k_r \sqrt{\frac{p_{SO_2}}{p_{SO_3}}} \left[p_{O_2} - \left(\frac{p_{SO_3}}{p_{SO_2} K_p} \right)^2 \right] \tag{A.1}$$

where p_i is the partial pressure of components, the reaction rate coefficient, k_r, is given by Fogler as [20]:

$$k_r = 9.8692 \cdot 10^{-3} \exp\left(\frac{-97782}{T} - 110.1 \ln T + 848.1 \right) \tag{A.2}$$

and the equilibrium constant, K_p, is:

$$K_p = 3.142 \cdot 10^{-3} \exp\left(\frac{98359}{RT} - 11.24 \right) \tag{A.3}$$

The heat capacity of each component in the considered temperature range is approximated by the experimental relation:

$$C_{p,i} = A_{C_{p,i}} + B_{C_{p,i}} T + C_{C_{p,i}} T^2 \tag{A.4}$$

where $A_{C_{p,i}}, B_{C_{p,i}}$ and $C_{C_{p,i}}$ are heat capacity coefficients. The heat of reaction is given by:

$$\Delta_r H = \sum_i \nu_i \Delta_f H_i^T \tag{A.5}$$

where $\Delta_f H_i^T$ is the enthalpy of formation of component i at a temperature T, which is given by:

$$\Delta_f H_i^T = \Delta_f H_i^{700} + A_{C_p}(T-700) + \frac{B_{C_p}}{2}(T^2-700^2) + \frac{C_{C_p}}{3}(T^3-700^3) \tag{A.6}$$

The reference temperature for the formation enthalpy is 700 K [6, 20]. Chemical data for the relevant chemical species are summarized in Table A.4.

The entropy of the gas stream is calculated according to:

$$S = \sum_i x_i \left(s_i^0 + \int_{298}^{T} \frac{C_{p,i}}{T} \mathrm{d}T \right) - R \sum_i x_i \ln x_i - R \ln \frac{p}{1.013 \cdot 10^5 \text{ Pa}} \tag{A.7}$$

where x_i is the mole fraction of component i, and s_i^0 is the standard entropy of component i summarized in Table A.4. If the equilibrium constant given by Fogler is used in the calculation of the Gibbs energy, the discrepancy between the total entropy production and the entropy balance may be as large as 6% [6]. Instead, Johannessen *et al.* used the following expression for the equilibrium constant:

$$K_p = \exp\left[\frac{-\Delta_r G^0(T)}{RT} \right] (1.1013 \cdot 10^5 \text{ Pa})^{-1/2} \tag{A.8}$$

where the standard Gibbs energy, $\Delta_r G^0$, is calculated using:

$$\Delta_r G^0 = \Delta_r H - T \Delta_r S \tag{A.9}$$

where $\Delta_r H$ is the heat of reaction and $\Delta_r S$ is the change in entropy of the reaction. The reaction quotient, Q_r, is calculated from:

$$Q_r = \prod_i p_i^{\nu_i} \tag{A.10}$$

where p_i is the partial pressure of component i. The reaction Gibbs energy is then [6]:

$$\Delta_r G = RT \ln \left(\frac{Q_r}{K_p} \right) \tag{A.11}$$

References

[1] A. Bejan, Entropy generation minimization: The new thermodynamics of finite-size devices and finite-time processes, Journal of Applied Physics 79 (3) (1996) 1191–1218.

[2] P. Salamon, A. Nitzan, B. Andresen, R. S. Berry, Minimum entropy production and the optimization of heat engines, Physical Review A 21 (6) (1980) 2115.

[3] E. Magnanelli, E. Johannessen, S. Kjelstrup, Entropy production minimization as design principle for membrane systems: Comparing equipartition results to numerical optima, Industrial & Engineering Chemistry Research 56 (16) (2017) 4856–4866.

[4] E. Johannessen, L. Nummedal, S. Kjelstrup, Minimizing the entropy production in heat exchange, International Journal of Heat and Mass Transfer 45 (13) (2002) 2649–2654.

[5] Ø. Wilhelmsen, E. Johannessen, S. Kjelstrup, Chapter 13. Entropy Production Minimization with Optimal Control Theory, The Royal Society of Chemistry, 2016, pp. 244–270.

[6] E. Johannessen, S. Kjelstrup, Minimum entropy production rate in plug flow reactors: An optimal control problem solved for SO_2 oxidation, Energy 29 (12-15) (2004) 2403–2423.

[7] E. Johannessen, S. Kjelstrup, A highway in state space for reactors with minimum entropy production, Chemical Engineering Science 60 (12) (2005) 3347–3361.

[8] L. Nummedal, S. Kjelstrup, M. Costea, Minimizing the entropy production rate of an exothermic reactor with a constant heat-transfer coefficient: the ammonia reaction, Industrial & engineering chemistry research 42 (5) (2003) 1044–1056.

Table A.4: Chemical data for components in the gas mixture [6, 20].

	SO_2	O_2	SO_3	N_2	Unit
$\Delta_f H^{700}$	$-2.78 \cdot 10^{-5}$	$0.12 \cdot 10^{-5}$	$-3.71 \cdot 10^{-5}$	$0.12 \cdot 10^{-5}$	J mol^{-1}
s^0	248.888	204.994	256.185	191.470	J K^{-1}mol^{-1}
A_{C_p}	30.178	23.995	35.634	26.159	J K^{-1}mol^{-1}
B_{C_p}	$42.452 \cdot 10^{-3}$	$17.507 \cdot 10^{-3}$	$71.722 \cdot 10^{-3}$	$6.615 \cdot 10^{-3}$	J K^{-2}mol^{-1}
C_{C_p}	$-18.218 \cdot 10^{-6}$	$-6.628 \cdot 10^{-6}$	$-31.539 \cdot 10^{-6}$	$-2.889 \cdot 10^{-7}$	J K^{-3}mol^{-1}
M_w	$64 \cdot 10^{-3}$	$32 \cdot 10^{-3}$	$80 \cdot 10^{-3}$	$28 \cdot 10^{-3}$	kg mol^{-1}

[9] S. Kjelstrup, E. Johannessen, A. Rosjorde, L. Nummedal, D. Bedeaux, Minimizing the entropy production of the methanol producing reaction in a methanol reactor, International Journal of Thermodynamics 3 (4) (2000) 147–153.

[10] A. Røsjorde, S. Kjelstrup, E. Johannessen, R. Hansen, Minimizing the entropy production in a chemical process for dehydrogenation of propane, Energy 32 (4) (2007) 335 – 343.

[11] L. Nummedal, A. Røsjorde, E. Johannessen, S. Kjelstrup, Second law optimization of a tubular steam reformer, Chemical Engineering and Processing: Process Intensification 44 (4) (2005) 429–440.

[12] R. Hånde, Ø. Wilhelmsen, Minimum entropy generation in a heat exchanger in the cryogenic part of the hydrogen liquefaction process: On the validity of equipartition and disappearance of the highway, International Journal of Hydrogen Energy.

[13] H. Serna, D. Barragán, Patterns in nature: more than an inspiring design, Revista de la Academia Colombiana de Ciencias Exactas, Físicas y Naturales 41 (160) (2017) 349–360.

[14] I. L. C. Barroso, The ontogeny of nasal heat exchange structures in arctic artiodactyles, Master's thesis, UiT The Arctic University of Norway (2014).

[15] E. Magnanelli, Ø. Wilhelmsen, M. Acquarone, L. P. Folkow, S. Kjelstrup, The nasal geometry of the reindeer gives energy-efficient respiration, Journal of Non-Equilibrium Thermodynamics 42 (1) (2017) 59–78.

[16] M.-O. Coppens, A nature-inspired approach to reactor and catalysis engineering, Current Opinion in Chemical Engineering 1 (3) (2012) 281–289.

[17] M. A. Gjennestad, E. Aursand, E. Magnanelli, J. Pharoah, Performance analysis of heat and energy recovery ventilators using exergy analysis and nonequilibrium thermodynamics, Energy and Buildings 170 (2018) 195–205.

[18] E. Johannessen, S. Kjelstrup, Entropy production rate minimization in plug flow reactor: Theoretical limit and practical approximation, Proc. ECOS 2002, Institute for Energy Engineering,TU Berlin (2002) 1352–1360.

[19] H. A. Jakobsen, Chemical reactor modeling, Springer, New York City, New York, 2014.

[20] H. S. Fogler, Essentials of Chemical Reaction Engineering, Pearson Education, London, England, 2010.

[21] S. Ergun, A. A. Orning, Fluid flow through randomly packed columns and fluidized beds, Industrial & Engineering Chemistry 41 (6) (1949) 1179–1184.

[22] J. A. E. Bryson, Y.-C. Ho, Applied Optimal Control, Routledge, Abingdon-on-Thames, United Kingdom, 1975.

[23] D. E. Kirk, Optimal control theory: an introduction, Courier Corporation, Chelmsford, Massachusetts, 2012.

[24] S. Gheorghiu, S. Kjelstrup, P. Pfeifer, M.-O. Coppens, Is the lung an optimal gas exchanger?, in: Fractals in biology and medicine, Springer, 2005, pp. 31–42.